

Analyzing Cochlear High-frequency Amplification Through a Two-Dimensional Organ of Corti Micro-electro-mechanical Model

Wen Cai¹ and Karl Grosh^{1, 2, 3, a)}

¹⁾*Department of Mechanical Engineering, University of Michigan, G.G. Brown Building, 2350 Hayward St., Ann Arbor, MI 48109-2125, U.S.A.*

²⁾*Department of Biomedical Engineering, University of Michigan, 1107 Carl A. Gerstacker Building, 2200 Bonisteel, Blvd., Ann Arbor, MI 48109-2099, U.S.A.*

³⁾*Kresge Hearing Research Institute, 4605 Medical Science Unit II, Ann Arbor, MI 48109-5616, U.S.A.*

^{a)}*Corresponding author: grosh@umich.edu*

Abstract.

The outer hair cell (OHC) in the organ of Corti (OoC) is hypothesized to boost the cochlear responses through electromotility. This hypothesis has been challenged for decades because of the low-pass OHC transmembrane impedance (commonly represented by a resistor-capacitor (RC) circuit). In this study, we analyze an electro-mechanical model of the OoC to explore mechanisms capable of producing high-frequency amplification. By examining the responses, we find that the inertia-like tectorial membrane (TM) shear motion is crucial for the cochlear amplification function. Only when the TM shear motion is inertia-dominant, the amplification gain is critically determined by the structural parameters related to the TM bending motion. The optimal structural parameters may help achieve the high gain seen in the *in vivo* experiments even with the RC cut-off frequency far below the characteristic frequency. As discussed in recent literature, we also find that the RC filtering of the OHC is a feature of the response rather than some inherent “problem”. The coupling of the OHC electromotility to the TM motion may be crucial for the high-frequency amplification.

INTRODUCTION

The outer hair cell (OHC) converts the modulation of a resting electrical potential into cycle-by-cycle force generation to add mechanical energy to the cochlea, both sharpening the filtering of incoming pressure and increasing the gain [2, 4]. Yet, the mechanism by which the OHC contributes to amplification at high frequencies has been debated because the mechanoelectric transducer (MET) current-induced voltage at high frequencies is greatly reduced by the low-pass OHC transmembrane impedance [3, 13]. To better understand the high-frequency amplification mechanism, studies have focused on the OHC transmembrane impedance characterized by a resistor-capacitor (RC) circuit [6, 10, 13]. Johnson et al. found that the cut-off frequency of the impedance ($\sim 1/(2\pi RC)$) is much higher than the value adopted in the literature [7]. Other work has intimated that the cut-off frequency of the transmembrane impedance is less important than the capacitance value in amplifying signals [1, 14].

On the other hand, the inertia-like radial motion of the tectorial membrane (TM) is required to allow the OHC to transfer energy to the cochlear partition [5, 9]. Mathematical models have been proposed to examine the condition that maximizes the power transfer of the OHC to the surrounding micro-structures. Ó Maoiléidigh and Jülicher found that the cochlear partition operating in the proximity of a Hopf bifurcation enhances the energy injection and achieves the key properties of the cochlear amplifier [15]. Rabbitt and Bidone identified the optimal working condition to maximize the power conversion by assuming a coupling between the hair bundle motion and the TM motion [11]. On the basis of the previous findings, we establish a linearized two dimensional electro-mechanical mathematical model for the organ of Corti (OoC) based on our previous cochlear model [12] to further analyze the cochlear amplification at high frequencies to identify the importance of the TM bending-related parameters on the amplification.

TWO-DIMENSIONAL ELECTRO-MECHANICAL MODEL OF THE OOC

The OoC houses the mechanosensory cells to filter the responses and transit afferent acoustic information. When the acoustic wave propagates to the inner ear, a coupled fluid-structure wave propagates along the cochlea, a wave which is amplified through an OHC-mediated process. In this section, an electro-mechanical mathematical model of a

single cross-section of the OoC without a traveling wave is described to help understand the crucial roles of different components in response to a force applied to the BM.

Kinematics of the OoC

The kinematical model of the OoC is shown in Fig. 1 (a). The depth of the cochlear slice is $10 \mu\text{m}$. Here, the BM is modeled as a simply-supported beam vibrating in the y direction. The pillar cells (PCs) are assumed rigid and hence rotate about point A. The reticular lamina (RL) rotates rigidly around point C. The movement of the RL and BM elongates or contracts the OHCs in their length direction. The hair bundles of the three OHCs are assumed rigid and rotate synchronously around their roots. The HB rotation angle is assumed to be the same for the three OHCs. The length change of the three OHCs varies with the position, as dictated by the rigid body rotation and translation of the RL and the motion of the BM. The TM is assumed to have two degrees of freedom, a shear mode and a bending mode. The shear mode, u_{tms} , is the translation in the x' direction. The bending mode, u_{tmb} , represents the rotation around point H, and under small rotations is in the y' direction to represent the TM bending motion.

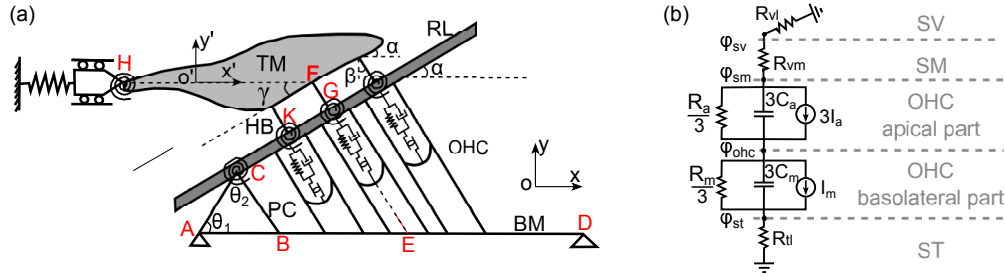


FIGURE 1. (a) Microstructures of the OoC. (b) Effective equivalent circuit for the OoC slice.

Using the kinematic relations among different components [12], the rotation of RL (Λ_{rl}), the rotation of HB (Λ_{hb}), and the length change of the second OHC (u_{ohc2}) are given by

$$\Lambda_{rl} = - \left[\frac{C_1}{L_{ro}} \frac{\cos(\theta_1 - \beta)}{\cos \Delta} + \frac{\psi_{ap}}{L_{pc}} \right] u_{bm} - \frac{C_2}{L_{ro}} u_{tms} + \frac{C_3}{L_{ro}} u_{tmb}, \quad (1)$$

$$\Lambda_{hb} = - \frac{C_1}{L_{st}} \left[\frac{\sin(\theta_1 - \alpha)}{\cos \Delta} - \frac{\cos(\theta_1 - \beta)}{\cos \Delta} \frac{L_{st}}{L_{ro}} \right] u_{bm} + \left[\frac{C_2}{L_{ro}} - \frac{\cos \gamma}{L_{st} \cdot \cos \Delta} \right] u_{tms} - \left[\frac{C_3}{L_{ro}} + \frac{\sin \gamma}{L_{st} \cdot \cos \Delta} \right] u_{tmb}, \quad (2)$$

$$u_{ohc2} = \left[C_1 \frac{\cos(\theta_1 - \beta)}{\cos \Delta} - C_1 \cos(\theta_1 - \alpha) + \psi_{ohc2} \cdot \cos \alpha \right] u_{bm} + C_2 u_{tms} - C_3 u_{tmb}, \quad (3)$$

where u_{bm} is the BM motion at point E (the location of the OHC 2 is assumed at the midpoint of the BM), u_{tmb} and u_{tms} are the TM bending motion and TM shear motion at point F. In the model, the counter-clockwise direction is defined as the positive direction for the rotations. The OHC contraction is considered as the positive OHC length change. The translation displacements u_{bm} is in the y -direction. As shown in Fig. 1 (a), points E and F are the connection points of the second OHC to the BM and TM, which are the points we use to represent the BM and TM transverse motion in experiments; θ_1 , θ_2 , α , γ , β are the angles shown in Fig. 1(a); Δ equals $\alpha - \beta$; L_{ro} is the distance between points C and G, L_{st} is the HB length, distance between points F and G; L_{pc} is the distance between points A and B; ψ_{ap} and ψ_{ohc} correspond to the values of the first mode shape of a simply supported beam evaluated at points B and E as $\psi_{ap} = \sin(\pi L_{pc}/b)$ and $\psi_{ohc2} = \sin(\pi L_{ohc2}/b)$. The length L_{ohc2} is the distance between points A and E while b is the length of the BM (the distance between points B and D). The constants C_1 , C_2 , and C_3 as:

$$C_1 = \psi_{ap} \sin(\theta_1 + \theta_2) / \sin \theta_2, \quad C_2 = \sin \gamma - \cos \gamma \cdot \tan \Delta, \quad C_3 = \cos \gamma - \sin \gamma \cdot \tan \Delta. \quad (4)$$

The expression of the length change of the second OHC can be used to compute the length changes of the first and third OHC, u_{ohc1} and u_{ohc3} using knowledge of u_{bm} , u_{tmb} and u_{tms} and the assumed BM mode shape [12].

Electro-mechanical coupling of the OHC

The electromechanical coupling in the OoC occurs through the variable mechanoelectrical-transducer (MET) conductance and the OHC electromotility. Here, we model the coupling for the second OHC. The variable MET conductance is a nonlinear function of the HB rotation. With the small rotation assumption, we adopt a linearized expression in Eq 5 to describe the current going through the apex of the OHC [12].

$$I_{hb} = Y_a V_{met} + \sigma_{met} L_{st} \Lambda_{hb} , \quad (5)$$

where Y_a is the apical admittance at the angular frequency ω , $Y_a = (1/R_a + i\omega C_a)$; R_a and C_a are the apical resistance and capacitance; σ_{met} is the MET sensitivity; V_{met} is the fluctuation of the potential about the resting potential across the OHC apex. The linearized MET current I_a is the HB rotation-induced current.

The OHC electromotility is a piezoelectric-like effect. Since the perturbation of the displacement and voltage away from equilibrium *in vivo* are typically small, the linear piezoelectric relations are employed to couple the electrical and mechanical properties as in Eqs. 6 and 7 [12].

$$F_{ohc} = K_{ohc} u_{ohc} + \epsilon_3 V_{ohc} , \quad (6)$$

$$I_{ohc} = V_{ohc} Y_m - \epsilon_3 \dot{u}_{ohc} , \quad (7)$$

where Y_m is the basolateral admittance at the angular frequency ω , $Y_m = (1/R_m + i\omega C_m)$; R_m and C_m are the basolateral resistance and capacitance; ϵ_3 is the electro-mechanical coupling; V_{ohc} is the fluctuation of the potential about the resting potential across the OHC basolateral membrane; K_{ohc} is the OHC stiffness.

Electrical model of the OoC

The equivalent circuit of the OoC cross-section is shown in Fig. 1 (b). The boundaries of SV and ST away from the BM are assumed to be nearly grounded. The potentials ϕ_{sv} , ϕ_{sm} , ϕ_{ohc} , and ϕ_{st} represent the variation of the voltage caused by the motion of the organ of Corti. Therefore, the potential across the OHC apical pole V_{met} is $\phi_{sm} - \phi_{ohc}$, and the potential across the OHC basolateral membrane V_{ohc} is $\phi_{ohc} - \phi_{st}$. The resistance R_{vl} is the resistance for current flowing from SV to ground; R_{vm} represents the resistance seen by the current flowing from the SV to the SM; R_{tl} is the resistance to current flow from ST to ground. For the electrical properties of the OHCs in the cross-section, we combine the effect of all three OHCs by multiplying the properties of the second OHC with 3 as in Fig. 1(b). Since the electromotility-induced current is a function of the OHC length change, the current I_m is described as

$$I_m = -\epsilon_3 (\dot{u}_{ohc1} + \dot{u}_{ohc2} + \dot{u}_{ohc3}) , \quad (8)$$

Based on Kirchhoff's laws, the governing equations for the given electrical circuit are written as

$$[-3Y_a(R_{vl} + R_{vm})/R_{tl} + 3Y_m]\phi_{st} - 3(Y_a + Y_m)\phi_{ohc} + 3I_a - I_m = 0 , \quad (9)$$

$$3Y_m\phi_{ohc} - (1/R_{tl} + 3Y_m)\phi_{st} + I_m = 0 , \quad (10)$$

For the model, the two unknowns for solving the electrical response of the OoC are ϕ_{ohc} and ϕ_{st} .

Dynamic model of the OoC

According to the kinematic relations shown above, the motion of the OoC can be represented by the three degrees of freedom, u_{bm} , u_{tms} , and u_{tmb} . To derive the governing equations for the three displacements, the Lagrange equation in Eq. 11 is employed.

$$\frac{\partial}{\partial t} \frac{\partial T}{\partial \dot{u}_j} + \frac{\partial L}{\partial u_j} = \frac{\partial \bar{Q}}{\partial u_j} , \quad (11)$$

where T and L , are, respectively the kinetic energy and potential energy; \bar{Q} represents the generalized work done by the external, viscous, and electromechanical forces; u_j represents the generalized coordinate, which is u_{bm} , u_{tms} , or

u_{tmb} ; the overdot represents the derivative with respect to time t . In the model, we treated the dissipative forces and the electromechanical coupling as external forces. Equivalently, we could have used the Rayleigh dissipation function for the viscous damping terms and included the piezoelectric coupling in the potential energy function.

For the microstructures shown in Fig. 1(a), the masses are assumed to be lumped into the BM (M'_{bm}) and TM (M'_{tms} and M'_{tmb}). To adjust the resonance of the cross section model to the characteristic frequency of the selected cochlear location, the fluid mass is added to increase the mass to M_{bm} for the BM motion and M_{tmb} for the TM bending motion. Therefore, the kinetic energy of the system is

$$T = \frac{1}{2}M_{bm}\dot{u}_{bm}^2 + \frac{1}{2}M_{tms}\dot{u}_{tms}^2 + \frac{1}{2}M_{tmb}\dot{u}_{tmb}^2. \quad (12)$$

The potential energy of the OoC is

$$L = \frac{1}{2}K_{bm}u_{bm}^2 + \frac{1}{2}K_{tms}u_{tms}^2 + \frac{1}{2}K_{tmb}u_{tmb}^2 + \frac{1}{2}K_{rl}\Lambda_{rl}^2 + \frac{3}{2}K_{hb}\Lambda_{hb}^2 + \frac{1}{2}K_{ohc}(u_{ohc1}^2 + u_{ohc2}^2 + u_{ohc3}^2), \quad (13)$$

where K_{bm} is the equivalent stiffness of the simply supported beam; K_{tms} and K_{tmb} are the stiffness of the TM shear and bending motion; K_{rl} is the rotational stiffness of RL at point C; K_{hb} is the rotational stiffness of the HB at point G. The stiffness K_{hb} and K_{ohc} are assumed to be the same for the three OHCs.

The generalized work done by the external force is

$$\begin{aligned} \bar{Q} = & -F_e(u_{ohc1} + u_{ohc2} + u_{ohc3}) + F_{ext} \cdot u_{bm} - C_{bm}\dot{u}_{bm}u_{bm} - C_{tms}\dot{u}_{tms}u_{tms} - C_{tmb}\dot{u}_{tmb}u_{tmb} \\ & - C_{sub}(L_{st}\dot{\Lambda}_{hb})(L_{st}\Lambda_{hb}) - C_{ohc}(\dot{u}_{ohc1}u_{ohc1} + \dot{u}_{ohc2}u_{ohc2} + \dot{u}_{ohc3}u_{ohc3}), \end{aligned} \quad (14)$$

where C_{bm} , C_{tms} , and C_{tmb} are the viscous damping coefficients respectively for the BM motion, TM shear motion, and TM bending motion. The viscous coefficient C_{sub} is introduced to simulate the damping force applied to the HB rotation mode, C_{ohc} corresponds to the viscous damping to impede the OHC length change; F_{ext} is the external force applied to point E to vibrate the basilar membrane; F_e is the force generated by the OHC electromotility, which is $F_e = \epsilon_3(\phi_{ohc} - \phi_{st})$ taken to be the same for each OHC.

Substituting Eqs. 12-14 into Eq. 11, we can derive the governing equations for the motions of the OoC. Together with the governing equations for the electrical domain (Eqs. 9 and 10), the micro-electro-mechanical model for the OoC is described as

$$\begin{bmatrix} M_s & O_{3 \times 2} \\ O_{2 \times 3} & O_{2 \times 2} \end{bmatrix} \begin{bmatrix} \ddot{\mathbf{u}} \\ \ddot{\boldsymbol{\phi}} \end{bmatrix} + \begin{bmatrix} C_s & C_{se} \\ C_{es} & C_e \end{bmatrix} \begin{bmatrix} \dot{\mathbf{u}} \\ \dot{\boldsymbol{\phi}} \end{bmatrix} + \begin{bmatrix} K_s & K_{se} \\ K_{es} & K_e \end{bmatrix} \begin{bmatrix} \mathbf{u} \\ \boldsymbol{\phi} \end{bmatrix} = \begin{bmatrix} \mathbf{F} \\ \mathbf{0} \end{bmatrix}, \quad (15)$$

where the matrix with the subscript s represents the mechanical properties, se represents the mechanical-electro coupling coefficients, es represents the electro-mechanical coupling coefficients, and e represents the electrical properties; the vector \mathbf{u} is $\mathbf{u} = [u_{bm} \ u_{tms} \ u_{tmb}]^T$; the vector $\boldsymbol{\phi}$ is $\boldsymbol{\phi} = [\phi_{ohc} \ \phi_{st}]^T$; the vector \mathbf{F} is $\mathbf{F} = [F_{ext} \ 0 \ 0]^T$; the vector $\mathbf{0}$ is a zero vector; the superscript T means the transpose of the vector; O represents a zero matrix, and the subscript indicates the size of the zero matrix.

By transforming the governing equations from the time domain into the frequency domain with a $e^{j\omega t}$ time dependence (e.g. $\mathbf{u} = \mathbf{U}e^{j\omega t}$, where \mathbf{U} represents the complex magnitude of the responses); the magnitude and phase of the mechanical and electrical responses can be calculated.

RESULTS

To analyze the high-frequency amplification, we choose a location where the characteristic frequency (CF) is around 13 kHz. Using the parameters listed in Tables I and II, Fig. 2 shows the model simulated amplitude and phase of u_{bm} , u_{tms} , and u_{tmb} in the frequency domain. The passive responses are calculated by setting the electro-mechanical coupling ϵ_3 to zero to simulate the responses of a dead cochlea. As shown in Fig. 2, the active peak amplitude of the BM is increased by around 8 times compared to the passive peak amplitude, although the OHC basolateral membrane cut-off frequency determined by $1/(2\pi R_m C_m)$ is 2 kHz, much lower than the CF. Since we only model the function of a slice of cochlea without the traveling wave, the phase accumulation effect is not present. The enhancement of the amplitude is not as high as 40 dB in the *in vivo* measurements. Yet, the simulated results share similarity with the *in vivo* results [8]. For example, the peak magnitude ratio of the active TM bending motion to the active BM motion is

around 3, and the peak magnitude ratio of the active TM shear motion to the active BM motion is around 0.7. The BM motion moves in phase with the TM bending motion, whereas the phase of the TM shear motion is around 90 degrees delayed compared to the BM motion at the peak frequency. The proposed model is able to qualitatively characterize the dynamics of the cochlea to analyze different amplification mechanisms.

TABLE I. Geometric and electric parameters

L_{ro}	L_{st}	L_{pc}	L_{ohc}	b	L_1	θ_1	θ_2	α	β	γ	R_m	C_m	R_a	C_a	R_{tl}	R_{vm}	R_{vl}
$[\mu m]$	$[\mu m]$	$[\mu m]$	$[\mu m]$	$[\mu m]$	$[\mu m]$	$[deg]$	$[deg]$	$[deg]$	$[deg]$	$[deg]$	$[M\Omega]$	$[pF]$	$[M\Omega]$	$[pF]$	$[M\Omega]$	$[M\Omega]$	$[M\Omega]$
39	2	33	51	102	10	66	62	12	12	15	28	18	37	1.3	0.4	2.5	1

TABLE II. Mechanical parameters and electromechanical coupling

K_{bm}	K_{tms}	K_{tmb}	K_{ohc}	K_{st}	K_{rl}	M_{bm}	M_{tms}	M_{tmb}	C_{bm}	C_{tms}	C_{tmb}	C_{sub}	C_{ohc}	ϵ_3	σ_{met}
$[\frac{N}{m}]$	$[\frac{N}{m}]$	$[\frac{N}{m}]$	$[\frac{N}{m}]$	$[\frac{nN \cdot \mu m}{radian}]$	$[\frac{nN \cdot mm}{radian}]$	$[ng]$	$[ng]$	$[ng]$	$[\frac{\mu N \cdot s}{m}]$	$[\frac{\mu N \cdot s}{m}]$	$[\frac{\mu N \cdot s}{m}]$	$[\frac{\mu N \cdot s}{m}]$	$[\frac{\mu N \cdot s}{m}]$	$[\frac{\mu N}{V}]$	$[\frac{A}{m}]$
0.45	0.08	0.05	0.02	69	60	53	27	15.5	0.1	0.4	0.1	0.19	0.175	-0.1	0.8

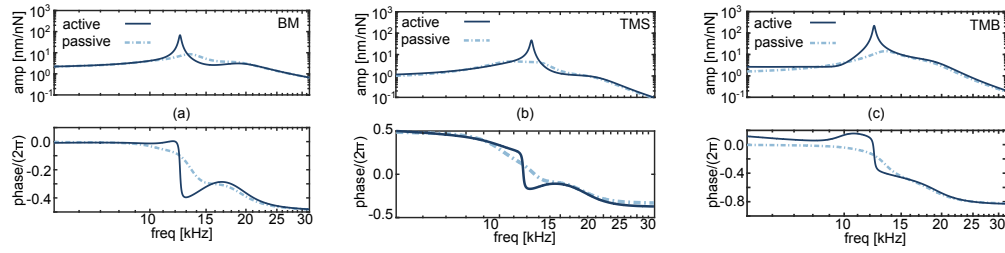


FIGURE 2. Amplitude and phase with respect to the applied force of (a) BM, (b) TMS, and (c) TMB responses.

Using the model in Eq. 15, we first find the poles of this 5th-order system. The poles of the system occur as 3 pairs of complex conjugates and 2 real-valued poles. Fig. 3(a) shows the three complex poles with a positive imaginary part (the complex poles with a negative imaginary part and the two real-valued poles are not shown.). The imaginary part of the pole indicates the natural frequency of the corresponding vibration mode. From Fig. 3 (a), the natural frequencies are slightly changed for the three vibration modes from the passive to the active case. In comparison, the damping ratio associated with pole 1 decreases substantially by the feedback control introduced by the OHC electromotility. The damping ratio can be estimated by $\cos(\Phi)$, where Φ is the angle subtended by the complex pole at the origin. In the figure, the damping ratio of pole 1 is decreased from 0.088 to 0.007 for $K_{tmb} = 50$ mN/m. Since pole 1 of the active case is the closest to the imaginary axis, the dynamics of the active system are dominated by pole 1.

By varying the dynamic parameters of the OoC, we find that the parameters associated with TM bending motion dominate the change of pole 1. Fig. 3(a) shows the poles by varying K_{tmb} from 40 mN/m to 85 mN/m. With the decrease of the stiffness, the angle Φ approaches 90° , which contributes to the increase of the BM gain as shown in Fig. 3(b). The BM active gain is defined as the active peak magnitude divided by the passive peak magnitude. When K_{tmb} is decreased to 40 mN/m, the real part of pole 1 is positive. The dynamics of the active system become unstable, which corresponds to the Hopf bifurcation identified in [15]. In addition, around the stability boundary, the active response is very sensitive to the parameters, as can be seen in Fig. 3(b) for the case shown with the solid line. The BM gain is increased by 10 times with a decrease of K_{tmb} from 48 mN/m to 42 mN/m.

With the parameters listed in Table II, the natural frequency of the TM shear motion ($\sqrt{K_{tms}/(4\pi^2 M_{tms})}$) is below the resonance of the system. The TM shear motion is inertia-like or mass-dominant around the resonance. We then decrease the TM shear-related mass M_{tms} by 10 times to set the shear motion to be stiffness-dominant around the resonance. As shown in Fig. 3(b), when the shear motion is stiffness-dominated ($M_{tms}/10$), the amplification gain is around 1, indicating almost no amplification happens in the system regardless of the change of K_{tmb} . This result is consistent with the finding in [5] that the inertia-like TM shear motion is fundamental for the cochlear amplification function.

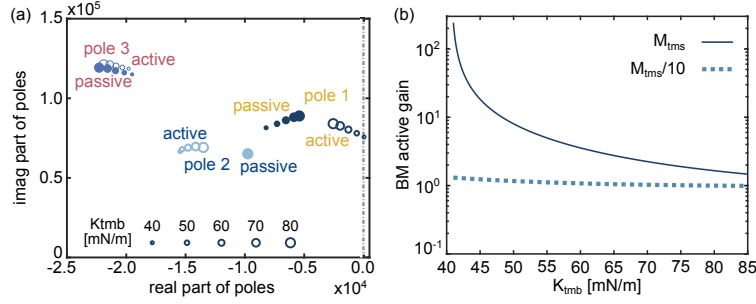


FIGURE 3. (a) Poles of the OoC system and (b) BM gain changing with K_{tmb} . As indicated in the inset of (a), the size of symbols in (a) represents the increase of K_{tmb} .

CONCLUSION

In the paper, we develop an electro-mechanical coupling model for the OoC to analyze the high-frequency amplification. The simulated active relative BM-TM motion at the resonance is similar to the *in vivo* experiment data. By evaluating the change of the poles, we find that the pole influenced most by the TM bending-related parameters dominates the dynamics of the active OoC. The decrease of the TM bending stiffness may help the system achieve the high gain seen in the *in vivo* experiments even with a low RC cut-off frequency, only when the TM shear motion is inertia-like. In addition, the variation of the TM bending stiffness may change the stability of the system. The Hopf bifurcation may occur. When the system operates in the vicinity of the stability boundary, the responses are highly sensitive to the small parameter change. Therefore, the OHC amplification process is a coupling effect of the structural and electrical parameters. The low RC cut-off frequency in this simple model does not undermine the the electromechanical-feedback amplification of the model.

ACKNOWLEDGEMENT

This work was supported by National Institutes of Health grant NIDCD R01-04084.

REFERENCES

1. A. Altoè, K. K. Charaziak, and C. A. Spera. Dynamics of cochlear nonlinearity: Automatic gain control or instantaneous damping? *J. Acoust. Soc. Am.*, 142(6):3510–3519, 2017.
2. J. B. Dewey, A. Altoe, C. A. Spera, B. E. Applegate, and J. S. Oghalai. Cochlear outer hair cell electromotility enhances organ of corti motion on a cycle-by-cycle basis at high frequencies in vivo. *Proc. Natl. Acad. Sci. USA.*, 118(43), 2021.
3. J. E. Gale and J. F. Ashmore. The outer hair cell motor in membrane patches. *Pflügers. Arch. Eur. J. Physiol.*, 434:267–271, 1997.
4. K. Grosh, J. F. Zheng, Y. Zou, E. de Boer, and A. L. Nuttall. High-frequency electromotile responses in the cochlea. *J. Acoust. Soc. Am.*, 115(5):2178–2184, 2004.
5. A. W. Gummer, W. Hemmert, and H. P. Zenner. Resonant tectorial membrane motion in the inner ear: its crucial role in frequency tuning. *Proc. Natl. Acad. Sci. USA.*, 93(16):8727–8732, 1996.
6. K. H. Iwasa. Not so presto? outcomes of sluggish prestin in outer hair cells. *arXiv preprint arXiv*, page 2004.14932, 2020.
7. S. L. Johnson, M. Beurg, W. Marcotti, and R. Fettiplace. Prestin-driven cochlear amplification is not limited by the outer hair cell membrane time constant. *Neuron.*, 70(6):1143–1154, 2011.
8. H. Y. Lee, P. D. Raphael, A. Xia, J. Kim, N. Grillet, B.E. Applegate, A.K.E. Bowden, and J.S. Oghalai. Two-dimensional cochlear micromechanics measured in vivo demonstrate radial tuning within the mouse organ of corti. *J. Neurosci.*, 36(31):8160–8173, 2016.
9. A. Nankali, Y. Wang, C. E. Strimbu, E. S. Olson, and K. Grosh. A role for tectorial membrane mechanics in activating the cochlear amplifier. *Sci. Rep.*, 10(1):17620, 2020.
10. R. D. Rabbitt. The cochlear outer hair cell speed paradox. *Proc. Natl. Acad. Sci. USA.*, 117(36):21880–21888, 2020.
11. R. D. Rabbitt and T. C. Bidone. A parametric blueprint for optimum cochlear outer hair cell design. *J. R. Soc. Interface*, 20(199):20220762, 2023.
12. S. Ramamoorthy, N. V. Deo, and K. Grosh. A mechano-electro-acoustical model for the cochlea: response to acoustic stimuli. *J. Acoust. Soc. Am.*, 121(5):2758–2773, 2007.

13. J. Santos-Sacchi, K.H. Iwasa, and W. Tan. Outer hair cell electromotility is low-pass filtered relative to the molecular conformational changes that produce nonlinear capacitance. *J. Gen. Physiol.*, 151(12):1369–1385, 2019.
14. M. van der Heijden and A. Vavakou. Rectifying and sluggish: outer hair cells as regulators rather than amplifiers. *Hear. Res.*, 423:108367, 2022.
15. D. Ó Maoiléidigh and F. Jülicher. The interplay between active hair bundle motility and electromotility in the cochlea. *J. Acoust. Soc. Am.*, 128(3):1175–1190, 2010.

COMMENTS AND DISCUSSION

John Allen: I would like to make sure that I understand what you said, and I am pretty sure that I do. The first and most important point for me is the signal voltage inside the outer hair cell is being low-pass filtered by the membrane capacitance. And it is not arguable in my point of view. There is no signal energy at ten or twenty kilohertz because of this low-pass effect. And Joe Santos talks about this important issue. Is that correct?

Wen Cai: I agree that the voltage signal is low-pass filtered. At ten or twenty kilohertz, the voltage signal is highly decreased. But there is not enough experimental and theoretical evidence to say that there is no signal energy input. According to our model, at tens of kilohertz, there is sufficient energy injection from the coupling of the OHC electromotility and the TM motion. The cooperation of the entire cochlear system determines the total gain enhancement, not just the low-pass characteristic of the OHCs.

John Allen: You kind of got a strange situation where you have something fighting the idea of a cochlear amplifier. You did not mention it, it is very important that the membrane capacitance is not in there. Joe Santos has very important papers where he measured the membrane capacitance as nonlinear and voltage-dependent.

Wen Cai: We include the membrane capacitance in our model. Although the membrane capacitance is nonlinear and voltage-dependent, we linearized it in the model, considering that the variation of the voltage and motility away from equilibrium *in vivo* is small.

John Allen: One last little question: does the membrane capacitance go up or down if the cell is depolarized? What happens to the membrane capacitance, is it bigger or smaller?

Wen Cai: It is smaller when the cell is depolarized.

John Allen: So the cut-off frequency is changing in a nonlinear way.

Wen Cai: If we consider the voltage change over a very wide range, the membrane capacitance and the cut-off frequency change in a nonlinear way. However, in our model, we consider only small variations in voltage to simulate the *in vivo* working conditions. The membrane capacitance is linearized to characterize the dynamics of the system.

Dáibhid Ó Maoiléidigh: Very interesting that the poles nearest the bifurcation seem to be very sensitive to the TM bending and inertia. This seems to be consistent with something I found which was that the conditions to get the Hopf bifurcation in the hair bundle required that you had negative stiffness, basically a gating compliance. That is very big. You could overcome this limitation if you added an inertia element on top of the hair bundles. You no longer need negative stiffness, but you do need some nonlinear response. Do you think what you are seeing along with that idea?

Wen Cai: Yes, I have seen the same thing. In our model, the hair bundle stiffness is always positive. We need the inertia effect of the TM on top of the hair bundles and the electromotility of the OHCs to achieve the Hopf bifurcation. Since we are considering only small deviations in voltage and displacement from equilibrium to simulate *in vivo* working conditions, the nonlinearity of the OHCs is linearized for simplicity.

Kuni Iwasa: How TM moves against RL? Only perpendicularly to RL? Then how the fluid between them moves?

Wen Cai: The TM moves perpendicularly and parallel to the RL. In this single cross-section OoC model, the traveling wave is not included. We apply a force directly to the BM.

Kuni Iwasa: is subtectorial drag between the TM and RL considered?

Wen Cai: Yes, the subtectorial drag between the TM and RL is included in the model and is represented by C_{sub} in Eq. (14).

Kuni Iwasa: What is the source of elastic load applied to OHCs?

Wen Cai: In the model, the relative motion of the RL and BM generates the elastic force applied to the OHCs. We assume the Dieters cells are rigid.

George Samaras: How did you constrain the electrical parameters that you list in Table I?

Wen Cai: We directly estimated the electrical parameters from the reference (Corbitt, Farinelli, Brownell, and Farrell, Biophysical Journal, 2012).

George Samaras: The OHC cutoff frequency can be varied by changing either R_m and C_m , do you have any insight on how each affects the active response of the model?

Wen Cai: When the OHC cut-off frequency is far below the characteristic frequency, changes in R_m do not show a strong influence on the active responses. But a decrease of C_m can greatly increase the active gain, especially when the system works near the Hopf bifurcation.

George Samaras: Based on my understanding, you are able to demonstrate increased sensitivity in your active model (compared to the passive one) at frequencies higher than the cutoff frequency because the magnitude of the basolateral admittance (Y_m) is really what controls the gain enhancement, not the cutoff frequency. It could be interesting to show the effect of Y_m on the gain (by varying Y_m while keeping the cutoff frequency the same).

Wen Cai: The focus of this paper is on the influence of structural parameters on the active amplification effect, rather than on basolateral admittance. Our study reveals the critical impact of TM bending-related parameters on amplification, even with a very low RC cut-off frequency. From this finding, we aim to demonstrate that RC filtering of the OHC is a feature of the system rather than an inherent 'problem'. The coupling of OHC electromotility to TM motion is crucial for controlling gain enhancement.

Renata Sisto: I don't understand for what reason in the generalized work done by the external force Q you inserted, in addition to the dissipative forces and the pressure, also a term representing the work done by the OHC, i.e. $Q = -F_e(u_{ohc1} + u_{ohc2} + u_{ohc3})$.

Wen Cai: In the model, we consider the organ of Corti as the system. The electromechanical force F_e is generated by the interaction of the OHCs with the external electrical field. Therefore, the electromechanical force F_e is treated as an external force to calculate the generalized work done by the external electric field on the organ of Corti system. We certainly could have introduced the piezoelectric-like coupling as part of the free energy function (then these same terms would appear in the potential function directly).

Renata Sisto: In addition, I derived the equation of motion for the BM and for the TM in the vertical direction using your Lagrangian. I neglected the dissipative forces and focused my attention on the force exerted by the OHC. I calculated the force exerted on the BM and compared it to that exerted on the TM (relatively to the bending motion) but I found very different functional expression. In the following I reported the derivation of the equation of motion. Let me define:

$$Coe1 = C_1 \frac{\cos(\theta_1 - \beta)}{\cos \Delta} - C_1 \cos(\theta_1 - \alpha) + \psi_{ohc2} \cdot \cos \alpha. \quad (16)$$

so that the OHC deformation in Eq. (3) can be written as

$$u_{ohc2} = Coe1 \cdot u_{bm} + C_2 \cdot u_{tms} - C_3 \cdot u_{tmb}. \quad (17)$$

The governing equations for the transversal displacement of the BM and TM are

$$M_{bm} \ddot{u}_{bm} = -K_{bm} u_{bm} - K_{rl} \Lambda_{rl} \frac{\partial \Lambda_{rl}}{\partial u_{bm}} - 3K_{hb} \frac{\partial \Lambda_{hb}}{\partial u_{bm}} + F_{ext} - 3K_{ohc} \cdot u_{ohc2} \frac{\partial u_{ohc2}}{\partial u_{bm}} - 3F_e \frac{\partial u_{ohc2}}{\partial u_{bm}}, \quad (18)$$

$$M_{tmb} \ddot{u}_{tmb} = -K_{tmb} u_{tmb} - K_{rl} \Lambda_{rl} \frac{\partial \Lambda_{rl}}{\partial u_{tmb}} - 3K_{hb} \frac{\partial \Lambda_{hb}}{\partial u_{tmb}} - 3K_{ohc} \cdot u_{ohc2} \frac{\partial u_{ohc2}}{\partial u_{tmb}} - 3F_e \frac{\partial u_{ohc2}}{\partial u_{tmb}}, \quad (19)$$

by assuming the same deformation for the three OHCs.

From Eqs. 18 and 19, the OHC forces applied to the transversal direction of the BM and TM are respectively

$$F_{ohc}^{bm} = 3Coe1 \cdot K_{ohc} (Coe1 u_{bm} - C_3 u_{tmb}) - 3Coe1 \cdot F_e, \quad F_{ohc}^{tmb} = -3C_3 \cdot K_{ohc} (Coe1 u_{bm} - C_3 u_{tmb}) + 3C_3 \cdot F_e. \quad (20)$$

The F_{ohc}^{bm} seems to me quite different with respect to F_{ohc}^{tmb} . Maybe you impose $C_3 = Coe1$? Or there is something I'm missing?

Wen Cai: The derivation you did here is what we did to derive the governing equations in matrix form. The only difference is that we considered the different deformations of the three OHCs (making the assumption that all three OHCs deform the same is a reasonable simplification). To compare the OHC electromechanical force applied to the transverse motion of the BM (u_{bm} in the y-axis direction in Fig. 1(a)) and the TM bending direction (u_{tmb} in the y'-axis direction in Fig. 1(a)), please note the angles we showed in Fig. 1(a). Generally, $Coe1$ is not equal to C_3 except when $\alpha = \beta$ and $\gamma = \alpha$. In this special case, the TM transverse direction is the same as the BM transverse direction such that $Coe1 = \psi_{ohc2} \cdot \cos \alpha$ and $C_3 = \cos \gamma = \cos \alpha$. In our model, we assume $L_{ohc} = b/2$, so $\psi_{ohc2} = 1$. Therefore, for this special case, $Coe1$ is equal to C_3 . Otherwise, because of the the geometry, the OHC forces applied to the transverse motions of the BM and TM are different.